JVST A
Journal of Vacuum Science & Technology A

ARTICLE

avs.scitation.org/journal/jva

Thermal atomic layer etching of silicon nitride using an oxidation and "conversion etch" mechanism

Cite as: J. Vac. Sci. Technol. A 38, 022607 (2020); doi: 10.1116/1.5140481
Submitted: 27 November 2019 · Accepted: 27 January 2020 ·
Published Online: 14 February 2020

Aziz I. Abdulagatov and Steven M. George

AFFILIATIONS

Department of Chemistry, University of Colorado, Boulder, Colorado 80309-0215

Note: This paper is part of the Special Topic Collection Commemorating the Career of John Coburn.

ABSTRACT

Thermal atomic layer etching (ALE) of silicon nitride was achieved using sequential exposures of oxygen (O_2) or ozone (O_3), hydrofluoric acid (HF), and trimethylaluminum [TMA, $Al(CH_3)_3$]. Thermal Si_3N_4 ALE will be useful to etch Si_3N_4 in semiconductor, optoelectronic, and MEMS devices. Thermal Si_3N_4 ALE was performed with Si_3N_4 thin films deposited on silicon wafers using low pressure chemical vapor deposition. *In situ* spectroscopic ellipsometry (SE) was employed to monitor the changes in the Si_3N_4 film thickness as well as the SiO_2 layer thickness. The SE results at 290 °C yielded an Si_3N_4 etch rate of 0.25 Å/cycle with an O_2-HF-TMA reactant sequence using partial pressures of 250, 0.65, and 1.2 Torr for O_2, HF, and TMA, respectively. The O_2, HF, and TMA reactants were held statically at the indicated partial pressures for 10, 5, and 5 s, respectively. Larger etch rates were observed using O_3 instead of O_2 as the oxidant. A higher Si_3N_4 etch rate of 0.47 Å/cycle was measured at 290 °C using an O_3-HF-TMA reactant sequence at the same partial pressures and static exposure times as the O_2-HF-TMA sequence. The Si_3N_4 etch rate was observed to decrease at lower temperatures. An Si_3N_4 etch rate of 0.07 Å/cycle was measured at the lowest temperature of 210 °C using an O_3-HF-TMA reactant sequence. The Si_3N_4 surface roughness was reduced after Si_3N_4 ALE. The SiO_2 layer on Si_3N_4 could be removed using sequential HF and TMA exposures. These sequential HF and TMA exposures could also very slowly etch the Si_3N_4 substrate. The Si_3N_4 etch rate was dependent on the reaction sequence. When an O_3-TMA-HF sequence was employed with reactant partial pressures of 250, 0.65, and 1.2 Torr for O_3, HF, and TMA, respectively, the Si_3N_4 etch rate was 0.20 Å/cycle at 290 °C. Thermal Si_3N_4 ALE adds to the growing list of materials that can be etched with atomic layer control using thermal chemistry.

I. INTRODUCTION

Atomic layer etching (ALE) is typically based on two sequential, self-limiting surface reactions.[1,2] A schematic of a model ALE process is shown in Fig. 1. The first reaction typically modifies the surface by halogenation or oxidation. The second reaction then removes the modified surface species and produces volatile etching products. The sequential application of the surface modification and removal reactions leads to ALE.[1,2] There are two main versions of ALE based on either plasma ALE or thermal ALE.[2–4]

Plasma ALE is an established etching process that employs energetic ions or neutrals to remove the modified surface species by a sputtering process and produces anisotropic etching.[2] The origins of plasma ALE can be traced back to the pioneering work of John Coburn and Harold Winters on Si etching with XeF_2 and Ar^+ ions.[5] They observed a synergy in Si etching when the XeF_2 and Ar^+ ions were incident on the Si substrate at the same time.[6] They could have tried to convert their Si etching process to a plasma Si ALE process by performing sequential XeF_2 and Ar^+ ion exposures. However, self-limiting behavior would not have been observed because XeF_2 spontaneously etches silicon.[7] Subsequent work demonstrated plasma Si ALE using halide adsorption and Ar^+ ion exposures.[8–11] Many other plasma ALE processes have also been developed for a variety of materials including SiO_2,[12,13] HfO_2,[14] InP,[15] Al_2O_3,[16] W,[17] Cr,[18] graphene,[19] and polymers.[20]

Thermal ALE is a newer etching process that utilizes thermal reactions to accomplish etching and achieves isotropic etching.[3,4,21,22] Isotropic etching is useful to conformally etch three-dimensional structures. Several different pathways have been documented for thermal ALE. One mechanism for thermal ALE utilizes

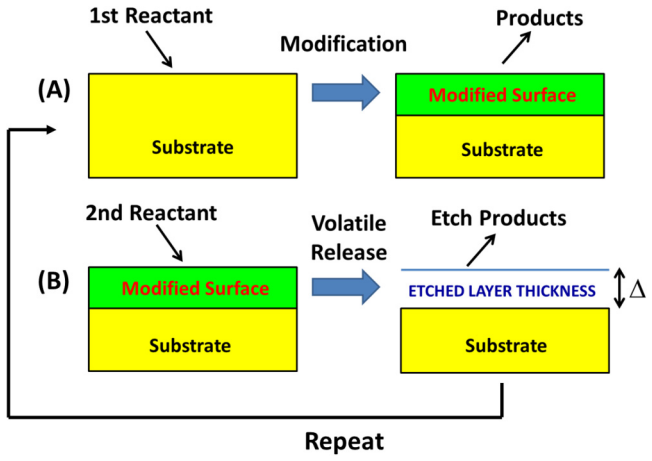

FIG. 1. Schematic for the generic ALE process based on two sequential reactions defined by (a) surface modification and (b) volatile release of the modified surface.

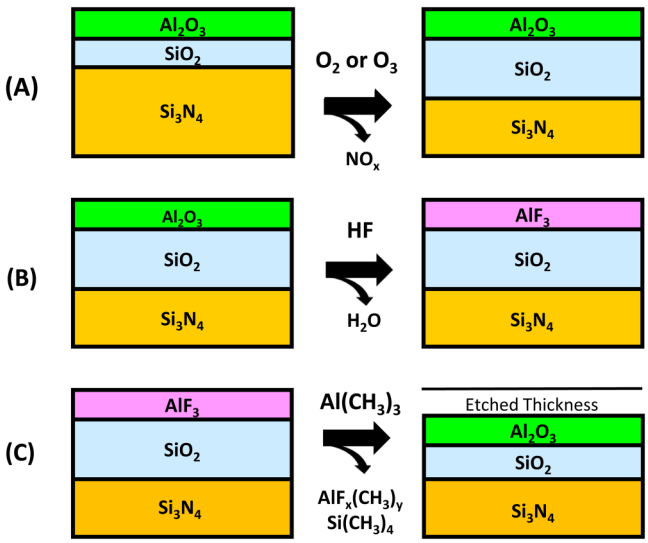

FIG. 2. Schematic for thermal Si_3N_4 ALE based on (a) oxidation by O_2 or O_3; (b) fluorination by HF; and (c) ligand-exchange and conversion with $Al(CH_3)_3$.

fluorination and ligand-exchange reactions.[3,4] This mechanism has been demonstrated for Al_2O_3,[4,21–28] HfO_2,[22,24,26,29] ZrO_2,[22,26] AlN,[30] GaN,[31] and VO_2.[23] Another pathway for thermal ALE involves conversion reactions that convert the initial material to a new material prior to etching. This conversion mechanism has been developed for ZnO,[32] SiO_2,[33] TiN,[34] W,[35] WO_3,[35] and Si ALE.[36]

In this paper, thermal Si_3N_4 ALE is demonstrated based on an oxidation and "conversion etch" mechanism. In similarity with earlier work on Si ALE,[36] Si_3N_4 is initially oxidized to SiO_2 using O_2 or O_3 as the oxidant. The SiO_2 layer can be converted to Al_2O_3 or an aluminum silicate using $Al(CH_3)_3$.[33] Hydrofluoric acid (HF) is able to fluorinate the aluminum to form AlF_3 or AlF_xO_y.[27] The aluminum fluoride layer is then reacted with $Al(CH_3)_3$ through a ligand-exchange reaction to form volatile $AlF(CH_3)_2$ products such as dimers of $AlF(CH_3)_2$ or $AlF(CH_3)_2$-$Al(CH_3)_3$.[25,37] A schematic of this mechanism is shown in Fig. 2 assuming conversion to Al_2O_3 and fluorination to AlF_3.

Thermal Si_3N_4 ALE is important because Si_3N_4 is a key material in semiconductor devices. Si_3N_4 is used as a spacer, mask, diffusion barrier, dielectric, and protection layer.[38] The etching of the silicon nitride spacer that forms the mask for implantation of source and drain and protects the gate sidewalls is one of the most challenging steps in semiconductor processing.[39] Si_3N_4 also has many other uses in optical and optoelectronic devices because of its wide bandgap.[38] In addition, Si_3N_4 is employed extensively in making MEMS devices.[40] Thermal Si_3N_4 ALE should yield isotropic etching that would be extremely valuable for fabricating advanced three-dimensional devices.[41]

Thermal Si_3N_4 ALE should also complement the plasma Si_3N_4 ALE methods. One plasma Si_3N_4 method is based on sequential hydrofluorocarbon plasma exposure and thermal annealing.[41–43] The second plasma Si_3N_4 ALE method is defined by sequential fluorocarbon plasma exposure and Ar^+ ion bombardment.[44–47] The third plasma Si_3N_4 ALE method is constructed from sequential hydrogen plasma exposure and fluorinated plasma exposure.[48–50] There are also variations of this third plasma Si_3N_4 ALE method where the reaction after the hydrogen plasma exposure involves either ion irradiation[51] or fluorinated plasma exposure followed by annealing.[39] The thermal Si_3N_4 ALE procedure developed in this paper is an isothermal process that avoids both plasma exposures and annealing steps.

II. EXPERIMENT

Thermal Si_3N_4 ALE was conducted in warm wall, hot-stage reactor.[36] A complete description of this apparatus has been given in a previous publication.[36] The walls of the reactor were maintained at 160 °C. The sample temperature was varied between 210 and 290 °C. The sample was held on the horizontal stage by gravity.

The reactor was equipped with an *in situ* spectroscopic ellipsometer (J.A.Woollam, model M-2000UI). This ellipsometer could monitor the changes in the Si_3N_4 film thickness and the SiO_2 layer thickness during Si_3N_4 ALE. The library files SiO2_JAW/Si3N4 (TaucLorentz)/INTRA_JAW(10 Å)/SiTempJAW were used to model the films during Si_3N_4 ALE. The Al_2O_3 layer is not explicitly considered because this layer is ultrathin and is merged with the SiO_2 layer. Ellipsometric measurements were recorded after each Si_3N_4 ALE cycle during the purging step.

One Si_3N_4 ALE cycle consisted of static exposures of O_2 or O_3, HF and trimethylaluminum (TMA) followed by a 30 s nitrogen purge time after each exposure. Static exposure times for O_2 or O_3, HF and TMA were 10, 5, and 5 s, respectively. Industrial grade O_2 (Airgas) was used to perform the oxidation. This O_2 was also the feed gas for the O_3 generator. O_3 was produced by an O3ONIA ozone generator (Switzerland) with an ozone output of ~15 wt. %

relative to O_2. HF was obtained from the HF vapor pressure above an HF-pyridine solution.[24] HF-pyridine (70 wt. %) and trimethylaluminum (97%) were supplied by Sigma-Aldrich.

The etch chamber was pumped with a mechanical pump (Alcatel Adixen 2010C1). The precursor dose valves, nitrogen feed mass flow controller, and the reactor isolation valve were closed simultaneously to achieve the static exposures. The reported reactant pressures refer to their partial pressures with respect to the background N_2 gas pressure of 1 Torr. Ultrahigh purity grade N_2 (99.9999%, Airgas) was used as the carrier gas.

The Si_3N_4 samples (University Wafer Inc.) were prepared using low pressure chemical vapor deposition of Si_3N_4 on silicon wafers. These low stress Si_3N_4 samples had an initial thickness of 100 nm. Rutherford backscattering spectroscopy analysis of the as-received samples confirmed Si-to-N ratios of 3-to-4. Forward recoil energy spectrometry also measured the hydrogen content of the Si_3N_4 films at <3 at. %. X-ray diffraction scans determined that the Si_3N_4 films were amorphous.

The silicon wafer coated with the Si_3N_4 film was cut into $2 \times 2\ cm^2$ coupons before use. Prior to Si_3N_4 ALE, the samples were dusted off using high purity nitrogen gas without using any solution-based cleaning. The nitride oxidation experiment was conducted using a solution pre-etched Si_3N_4 sample. For this purpose, the native oxide was removed using a 1 min dip in a 10 wt. % HF solution followed by rinsing in DI water.[52]

X-ray photoelectron spectroscopy (XPS) (PHI 5600, RBD Instruments) measured the film composition after the Si_3N_4 ALE process. A monochromatic Al Kα x-ray source (1486.6 eV) was used to collect survey scans with a pass energy of 93.9 eV and a step size of 0.400 eV. Auger Scan software package (Auger Scan, RBD Instruments) was employed to collect the data. Casa XPS software (Casa XPS, Casa Software) determined the surface concentrations using the peak areas and the corresponding sensitivity factors.

III. RESULTS AND DISCUSSION

A. Thermal Si_3N_4 ALE using O_2

Figure 3 displays the Si_3N_4 thickness change and corresponding thickness for the SiO_2 layer during Si_3N_4 ALE at 290 °C using O_2-HF-TMA sequential exposures. O_2, HF, and TMA were exposed at partial pressures of 250, 0.65, and 1.2 Torr, respectively. The etch temperature of 290 °C was chosen to avoid potential problems with TMA decomposition that may occur at higher temperatures.[53,54] Figure 3 shows that the Si_3N_4 thickness change occurs at a rate of 0.25 Å/cycle. In addition, the SiO_2 layer levels off at a thickness of ~9 Å after 40 Si_3N_4 ALE cycles.

For comparison, crystalline silicon can be etched at a higher etch rate of 0.45 Å/cycle using similar reactant conditions at 290 °C.[36] The lower etch rate for Si_3N_4 probably arises from the difference in oxidation rates for silicon and silicon nitride. The oxidation rate of Si_3N_4 CVD films in dry and wet oxygen ambient is much lower than the oxidation rate for Si.[55–58] The lower oxidation rate of Si_3N_4 limits Si_3N_4 oxidation and reduces the Si_3N_4 etch rate.

Previous studies have observed that higher O_2 pressures lead to larger Si_3N_4 oxidation rates.[58] In an attempt to increase the Si_3N_4 etch rate, higher O_2 pressures of 350 and 450 Torr were used with the same temperature, HF and TMA partial pressures, reactant sequence, and exposure times as in Fig. 3. Figure 4 shows that the increase in O_2 pressure resulted in only a slight increase in the Si_3N_4 etch rate from 0.25 Å/cycle at 250 Torr to 0.28 Å/cycle at 450 Torr. This result suggested that a more powerful oxidizing agent is needed to increase the Si_3N_4 oxidation rate and the Si_3N_4 etch rate. Several studies have reported that Si_3N_4 has a significantly higher oxidation rate in H_2O than in O_2.[55,56] In addition, thermochemical calculations indicate that ozone (O_3) can be more favorable for Si_3N_4 oxidation.[59]

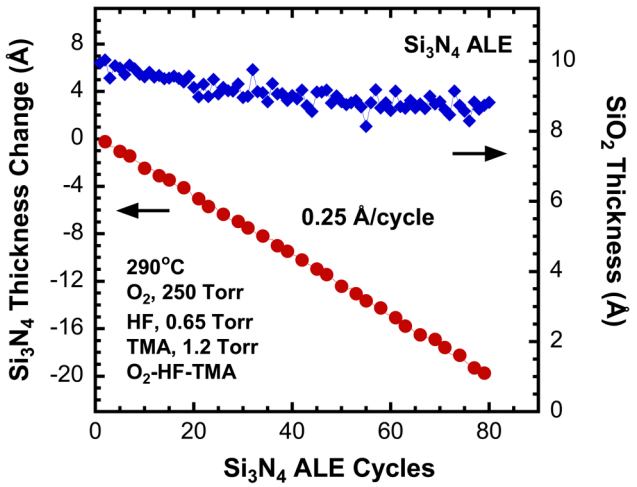

FIG. 3. Si_3N_4 thickness change and SiO_2 film thickness vs number of ALE cycles during Si_3N_4 etching using O_2-HF-TMA reactant sequence at 290 °C.

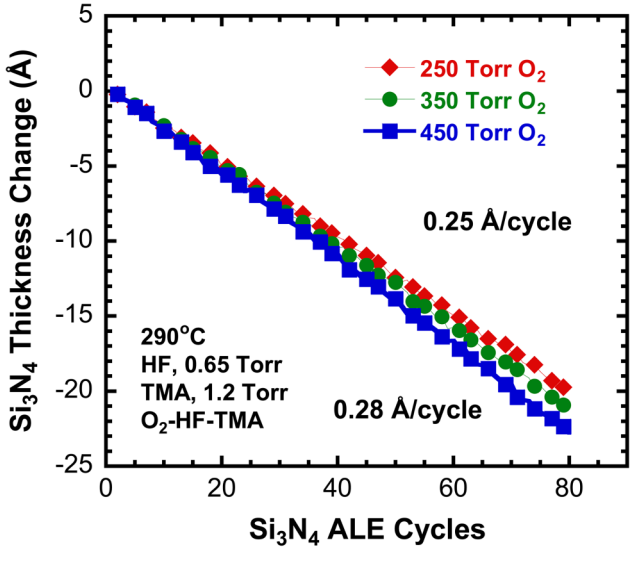

FIG. 4. Si_3N_4 thickness change vs number of ALE cycles at different O_2 pressures using O_2-HF-TMA reactant sequence at 290 °C.

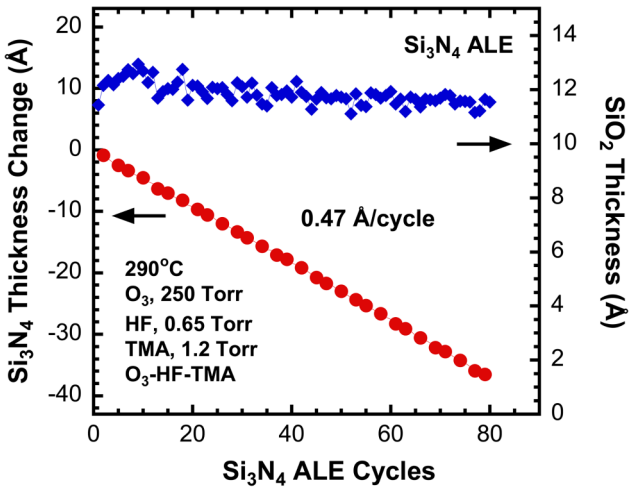

FIG. 5. Si_3N_4 thickness change and SiO_2 film thickness vs number of ALE cycles during Si_3N_4 etching using O_3-HF-TMA reactant sequence at 290 °C.

B. Thermal Si_3N_4 ALE using O_3

Figure 5 shows the Si_3N_4 thickness change and values for the SiO_2 layer thickness versus number of ALE cycles at 290 °C using an O_3-HF-TMA reactant sequence. Partial pressures for O_3, HF, and TMA were 250, 0.65, and 1.2 Torr, respectively. O_3 was held statically for 10 s. HF and TMA were held statically for 5 s. The Si_3N_4 film thickness is etched at an etch rate of 0.47 Å/cycle.

The etch rate of 0.47 Å/cycle using O_3 is higher than the etch rate of 0.25 Å/cycle using O_2 as observed in Fig. 3. In addition, the etch rate of 0.47 Å/cycle is comparable with the etch rate of 0.45 Å/cycle observed for Si ALE using the O_3-HF-TMA sequence at similar reaction conditions.[60] Figure 5 also reveals that the SiO_2 layer thickness is fairly constant at ~11 Å during the 80 Si_3N_4 ALE cycles. This SiO_2 thickness of ~11 Å using O_3 is higher than the SiO_2 thickness of ~9 Å using O_2 as observed in Fig. 3.

C. Effect of reactant pressure on etch rate

Figure 6 displays the dependence of the Si_3N_4 etch rate on TMA and HF partial pressures at 290 °C. Figure 6(a) shows the Si_3N_4 etching as the TMA pressure is varied from 0.6 to 1.9 Torr with the O_3 and HF pressures held constant at 250 and 0.65 Torr, respectively. The Si_3N_4 etch rate increased from 0.38 Å/cycle to 0.47 Å/cycle as the TMA pressure increased from 0.6 Torr to 1.2 Torr. The TMA pressure increase from 1.2 to 1.9 Torr did not increase the etch rate. At both pressures, the etch rate stayed constant at 0.47 Å/cycle. In comparison, the Si etch rate during Si ALE was also larger at higher TMA pressures. The Si etch rate increased from 0.2 Å/cycle at a TMA pressure of 30 Torr to 0.4 Å/cycle at a TMA pressure of 250 Torr.[36]

Figure 6(b) shows the Si_3N_4 etching at 290 °C as the HF pressure is varied from 0.40 to 0.81 Torr with the O_3 and TMA pressures held constant at 250 and 1.2 Torr, respectively. The increase in HF pressure from 0.40 to 0.65 Torr resulted in an increase in the etch rate from 0.40 to 0.47 Å/cycle. Further increase in the HF pressure from 0.65 to 0.81 Torr resulted in a slight increase from 0.47 to 0.50 Å/cycle. In comparison, the Si etch rate was constant at 0.4 Å/cycle at HF pressures from 0.5 Torr to 1.5 Torr.[36]

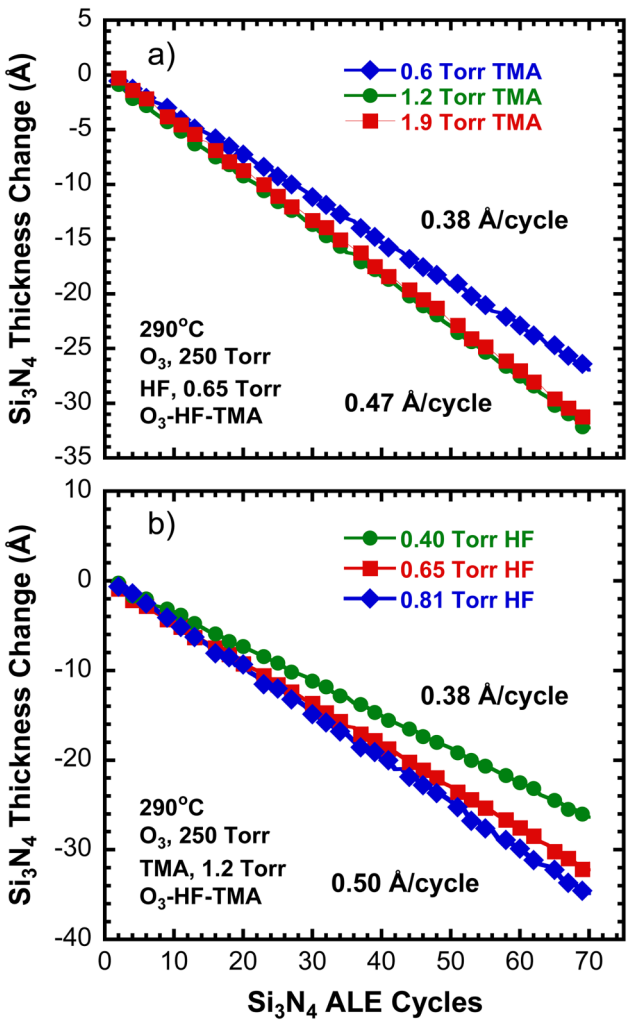

FIG. 6. Si_3N_4 thickness change vs number of ALE cycles for (a) various TMA pressures and (b) various HF pressures. Si_3N_4 etching was conducted at 290 °C using O_2-HF-TMA reactant sequence.

Slightly higher Si_3N_4 etch rates are expected at higher TMA and HF pressures. Higher TMA pressures lead to more conversion of SiO_2 to Al_2O_3.[33] Higher HF pressure is also known to yield larger fluorination thicknesses and higher Al_2O_3 etch rates.[27] The TMA and HF pressures also have little effect on the SiO_2 thickness. The SiO_2 thickness remained constant at ~11–13 Å independent of TMA pressure during the experiments shown in Fig. 6(a). The SiO_2 thickness increased slightly from ~12 Å at an HF pressure of 0.65 Torr to ~16 Å at an HF pressure of 0.40 Torr during the experiments shown in Fig. 6(b). These SiO_2 thicknesses are approximate because the measurements of SiO_2 thickness may be affected by surface roughness.[61,62]

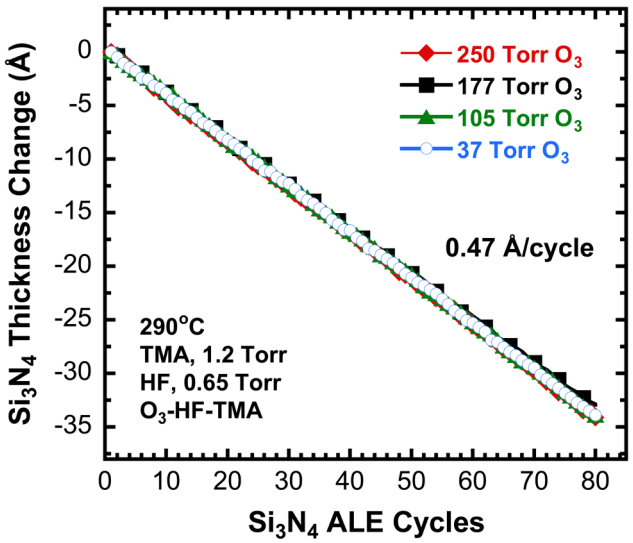

FIG. 7. Si_3N_4 thickness change vs number of ALE cycles for various O_3 pressures using O_3-HF-TMA reactant sequence at 290 °C.

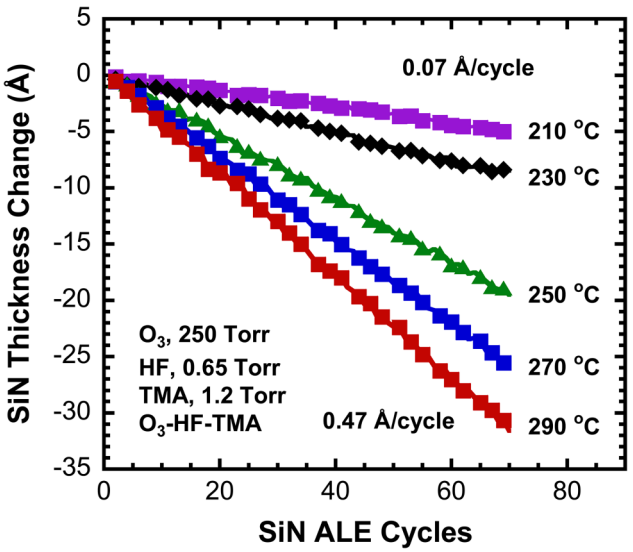

FIG. 8. Si_3N_4 thickness change vs number of ALE cycles at various temperatures using O_3-HF-TMA reactant sequence at 290 °C.

In contrast to the dependence of the Si_3N_4 etch rate on TMA and HF pressure, there is no observable dependence of the Si_3N_4 etch rate on the O_3 pressure. Figure 7 shows the dependence of the Si_3N_4 etch rate on O_3 pressure at 290 °C. The partial pressures of TMA and HF were fixed at 1.2 and 0.65 Torr, respectively, as the O_3 pressure was varied from 37 to 250 Torr. These results illustrate that the Si_3N_4 etch rate is independent of the O_3 pressure. This behavior suggests that O_3 is a powerful oxidation agent. O_3 is able to produce enough Si_3N_4 oxidation to maintain high Si_3N_4 etch rates even at lower O_3 pressures. The SiO_2 thickness also stayed constant at ~12 Å over the 80 Si_3N_4 ALE cycles for each O_3 pressure. These results argue that the oxidation of Si_3N_4 by O_3 is self-limiting.

D. Temperature dependence of etch rate

Figure 8 shows the Si_3N_4 thickness changes for sample temperatures of 210, 230, 250, 270, and 290 °C. These experiments were conducted using the O_3-HF-TMA reactant sequence and partial pressures of 250, 0.65, and 1.2 Torr, for O_3, HF, and TMA, respectively. The Si_3N_4 etch rate increases from 0.07 Å/cycle at 210 °C to 0.47 Å/cycle at 290 °C. This trend is consistent with a thermally activated process. An Arrhenius plot of the temperature-dependent Si_3N_4 etch rates is shown in Fig. 9. This Arrhenius plot yields an activation barrier of $E_a = 13.4$ kcal/mol for the combined oxidation, conversion, fluorination, and ligand-exchange reactions.

E. Surface roughness and composition after etching

Figure 10 displays AFM results for the as-received and etched Si_3N_4 substrates. Si_3N_4 ALE was performed at 290 °C using an O_3-HF-TMA reactant sequence with pressures of 250, 0.65, and 1.2 Torr for O_3, HF, and TMA, respectively. Figure 10(a) indicates that the root-mean-square (RMS) surface roughness of the as-received Si_3N_4 substrate is 4.7 Å ± 0.2. After 100 cycles of Si_3N_4 ALE, Fig. 10(b) reveals that the RMS surface roughness decreased to 3.1 Å ± 0.2.

The results in Fig. 10(b) demonstrate that the Si_3N_4 ALE process smoothens the surface of the Si_3N_4 film. Surface smoothing by thermal ALE processes have been previously reported for a number of systems including Al_2O_3 ALE (Refs. 4 and 21)

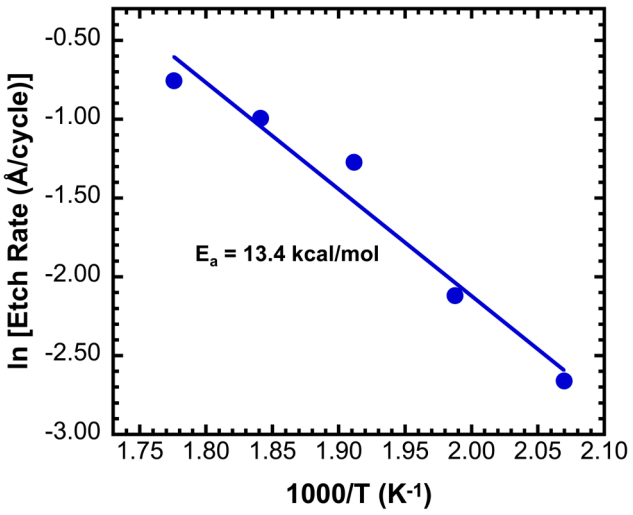

FIG. 9. Arrhenius plot of the temperature-dependent Si_3N_4 etch rates. Slope of the Arrhenius plot yields an activation barrier of $E_a = 13.4$ kcal/mol.

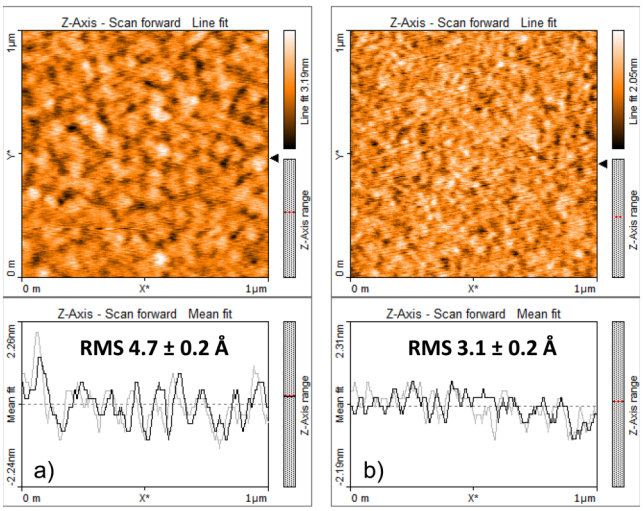

FIG. 10. AFM images of Si_3N_4 sample surface (a) prior and (b) after 100 cycles of ALE performed using the O_3-HF-TMA reactant sequence at 290 °C.

and HfO_2 ALE.[24] No increase in surface roughness was observed for thermal Si ALE at higher O_2 pressures of 250 Torr at 290 °C.[36]

Figure 7 shows that the O_3 pressure can be reduced from 250 to 37 Torr without affecting the Si_3N_4 etch rate. However, a low O_3 pressure of 37 Torr did not significantly reduce the surface roughness. The RMS roughness after 100 Si_3N_4 ALE cycles using an O_3 pressure of 37 Torr was 4.3 Å. This roughness is only slightly less than the RMS surface roughness of 4.7 Å for the as-received substrate. The surface smoothing is dependent on the O_3 pressure. Higher pressures of O_3 may produce more uniform SiO_2 films that yield surface smoothing during Si_3N_4 ALE.

XPS analysis was used to quantify the species on the Si_3N_4 surface after Si_3N_4 ALE. An XPS scan of the Si_3N_4 surface was performed after 100 Si_3N_4 ALE cycles using an O_3-HF-TMA reactant sequence with the partial pressures of 250, 0.65, and 1.2 Torr, respectively, at 290 °C. After the Si_3N_4 ALE ending with a TMA exposure and subsequent atmospheric exposure, the compositions from XPS were: 37.2 at. % (Si-2p); 28.9 at. % (N-1s); 19.1 at. % (O-1s); 10.9 at. % (C-1s); 2.8 at. % (Al-2p); and 1.2 at. % (F-1s).

Oxygen is attributed to remaining SiO_2 and Al_2O_3 from O_3 exposure and conversion during Si_3N_4 ALE. In addition, additional oxygen may be produced from Si_3N_4 oxidation resulting from atmospheric exposure. The aluminum results from the conversion of SiO_2 to Al_2O_3 during the TMA reaction.[33] Adventitious carbon is present due to ambient air exposure when transferring from the ALE reactor to the XPS chamber for analysis.

F. Removal of residual surface oxide

The Si_3N_4 ALE process produces an SiO_2 layer when Si_3N_4 is oxidized by O_2 or O_3 as shown in Fig. 2. This SiO_2 layer remains on the Si_3N_4 film during and after etching. Some applications may benefit from the removal of this SiO_2 layer. The SiO_2 layer can be removed from the Si_3N_4 surface by performing SiO_2 ALE. An earlier study has characterized SiO_2 ALE at 300 °C with TMA and HF as the reactants.[33]

Figure 11 shows the Si_3N_4 thickness change and the SiO_2 layer thickness during Si_3N_4 ALE followed by SiO_2 ALE at 290 °C. Si_3N_4 ALE was conducted for the first 40 cycles using an O_3-HF-TMA reactant sequence with O_3, HF, and TMA pressures of 250, 0.65, and 0.7 Torr, respectively. Subsequently, SiO_2 ALE was performed for the next 80 cycles using an HF-TMA reactant sequence.[33] The only difference between the Si_3N_4 ALE process and the SiO_2 ALE process was the omission of the O_3 exposure during SiO_2 ALE.[33]

Figure 11 reveals that the first 15 cycles of SiO_2 ALE decrease the SiO_2 layer thickness from 14 Å to a thickness of 7.5 Å. This apparent SiO_2 thickness then remains constant during the next 65 cycles. The apparent SiO_2 thickness from ellipsometry analysis may be associated with surface roughness instead of a true SiO_2 film thickness.[61,62] Atomic force microscope images are needed to distinguish between surface roughness and a true film thickness for these ultrathin film thicknesses.

There is also a slow reduction of the Si_3N_4 film thickness during SiO_2 ALE. An Si_3N_4 etch rate of 0.05 Å/cycle is observed from the HF-TMA reactant sequence at 290 °C. In contrast, no etch of Si was observed when the same SiO_2 ALE approach was applied to remove SiO_2 after thermal Si ALE using O_3-HF-TMA. The slow etch of Si_3N_4 during the HF-TMA reactant exposure is believed to proceed through TMA conversion of Si_3N_4 to AlN. The HF then fluorinates the AlN to AlF_3 prior to the removal of AlF_3 by a ligand-exchange reaction with the subsequent TMA exposure.

In the Si_3N_4 ALE process using HF and TMA, the TMA exposure would play the dual role of converting the Si_3N_4 surface to

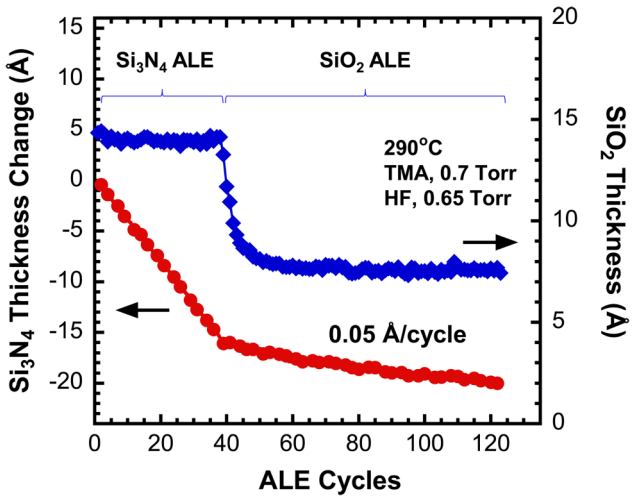

FIG. 11. Si_3N_4 thickness change and SiO_2 thickness vs first 40 cycles of Si_3N_4 ALE using O_3-HF-TMA reactant sequence followed by SiO_2 ALE using sequential HF and TMA exposures at 290 °C.

AlN and then removing AlF_3 during a ligand-exchange reaction. Thermochemical calculations show that both conversion and fluorination reactions are feasible because the standard free energy changes are negative:[59]

$$Si_3N_4 + 4Al(CH_3)_3\ (g) \rightarrow 4AlN + 3Si(CH_3)_4\ (g) \quad \Delta G^\circ(290^\circ C) = -358\ \text{kcal},$$
$$AlN + 3HF\ (g) \rightarrow AlF_3 + NH_3\ (g) \quad \Delta G^\circ\ (290^\circ C) = -62\ \text{kcal}.$$

The Si_3N_4 etch rate may be increased at larger partial pressures of HF and TMA. Figure 12 shows the results for Si_3N_4 ALE at a higher HF pressure of 1.6 Torr with TMA pressures of 2 and 3 Torr. The higher pressures of HF and TMA only result in marginal increases in the Si_3N_4 etch rate from 0.05 to 0.06 Å/cycle. These results indicate that the oxidation step with O_3 is critical to obtain higher Si_3N_4 etch rates.

G. Effect precursor exposure sequence

The precursor exposure sequence can affect Si_3N_4 ALE. The O_3-HF-TMA exposure sequence yields an Si_3N_4 etch rate of 0.47 Å/cycle at 290 °C as shown in Fig. 5. Experiments were conducted to determine the effect of changing the precursor exposure sequence to O_3-TMA-HF. Figure 13 shows the Si_3N_4 thickness change and SiO_2 layer thickness versus number of ALE cycles at 290 °C for the O_3-TMA-HF exposure sequence. The Si_3N_4 ALE was conducted using O_3, HF, and TMA pressures of 250, 0.65, and 1.2 Torr, respectively. The O_3-TMA-HF exposure sequence leads to a reduction in the Si_3N_4 etch rate to 0.20 Å/cycle at the same reactant pressures used for the O_3-HF-TMA exposure sequence.

The reduction in the Si_3N_4 etch rate occurs when the TMA is after the O_3 exposure rather than after the HF exposure. The TMA exposure after the O_3 exposure may lead to Al_2O_3 growth on the substrate. This extra Al_2O_3 may act as a diffusion barrier and restrict the oxidation of silicon during the O_3 exposure. The results for the SiO_2 thickness in Fig. 13 support this explanation. The SiO_2 thickness increases from the initial value of 11 Å over the first 60–70 ALE cycles. The SiO_2 thickness reaches a maximum value of 41 Å after about 80 cycles and then slowly reduces to 39 Å after 160 ALE cycles. The Al_2O_3 growth is included in the SiO_2 thickness because there is no separate Al_2O_3 layer included in the ellipsometry model. In comparison, the SiO_2 layer had a thickness of only 11 Å using the O_3-HF-TMA exposure sequence.

Similar behavior was observed for Si ALE when the reactant exposure sequence was changed from O_2-HF-TMA to O_2-TMA-HF for the same reactant pressures at 290 °C.[36] The Si etch rate was 0.4 Å/cycle for the O_2-HF-TMA exposure sequence. The Si etch rate decreased to 0.2 Å/cycle for the O_2-TMA-HF exposure sequence. These Si etch rates were measured at 290 °C with pressures of 250, 1, and 1 Torr for O_2, HF, and TMA, respectively.[36] The decrease in the

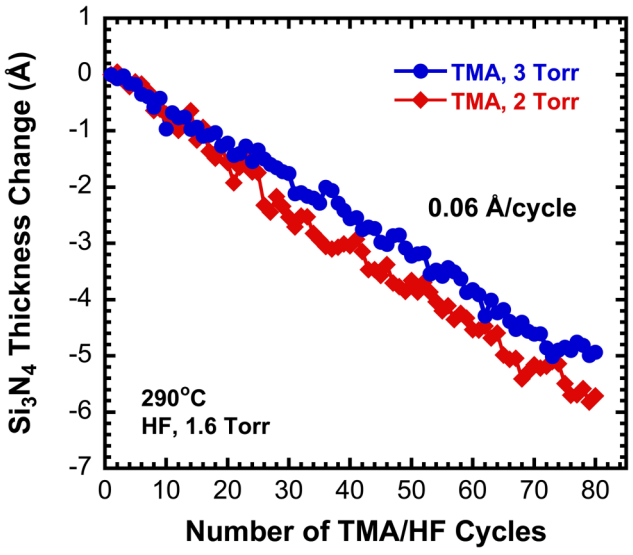

FIG. 12. Si_3N_4 thickness change vs number of ALE cycles using sequential HF and TMA exposures at 290 °C.

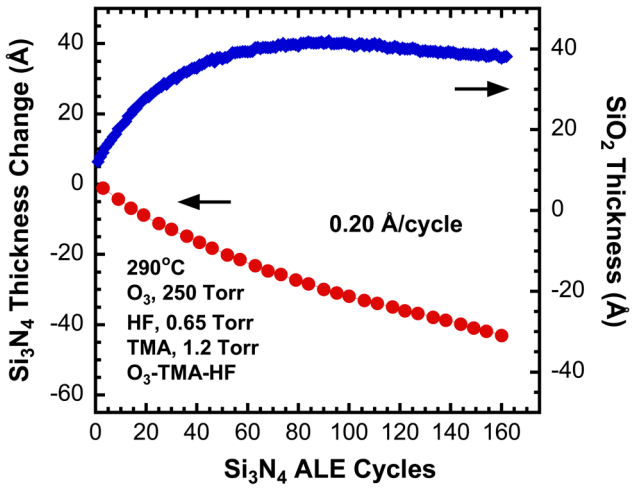

FIG. 13. Si_3N_4 thickness change and SiO_2 thickness vs number of ALE cycles for Si_3N_4 etching using O_3-TMA-HF reactant sequence at 290 °C.

Si etch rate was also attributed to Al_2O_3 deposition occurring when TMA follows the O_2 exposure.

H. Si_3N_4 oxidation by O_3

Si_3N_4 oxidation has predominantly been studied at high temperatures of 900–1400 °C using O_2 and H_2O as the oxidation reactants.[55–58,63] Si_3N_4 is very resistant to oxidation and is known to form a thin graded oxidized nitride layer between the film surface and the underlying nitride.[63] In addition, very little is known about Si_3N_4 oxidation at lower temperatures with any oxidation reactant.[63] To our knowledge, no studies have reported the oxidation of Si_3N_4 with ozone. Because O_3 has been employed as the oxidation reactant in these studies of Si_3N_4 ALE, additional experiments were performed to characterize the oxidation of Si_3N_4 after multiple O_3 exposures at 290 °C.

Figure 14 shows change in SiO_2 thickness versus number of O_3 exposures at 290 °C using an O_3 pressure of 250 Torr for 10 s. There was a 30 s purge time between the O_3 exposures. Ellipsometric measurements were performed after each O_3 exposure during the purge step. Prior to this oxidation, the Si_3N_4 sample was dipped in an aqueous HF solution to remove the native oxide. Figure 14 shows a rapid increase in SiO_2 thickness from 5 to 6.5 Å on the first O_3 exposure. The SiO_2 thickness then continues to increase to ~9 Å after 10 O_3 exposures. The SiO_2 thickness then grows slowly with O_3 exposures and reaches a thickness of ~10 Å after 40–50 O_3 exposures.

The apparent initial SiO_2 thickness of 5 Å on Si_3N_4 is attributed to surface roughness after the HF etching rather than a true oxide thickness. Similar behavior was observed during spectroscopic ellipsometry studies on Si surfaces where surface roughness leads to an apparent surface oxide thickness.[61,62] An apparent initial surface oxide was also measured during spectroscopic ellipsometry experiments of the oxidation of a wet-etched silicon-on-insulator wafer using O_2 at 290 °C.[36]

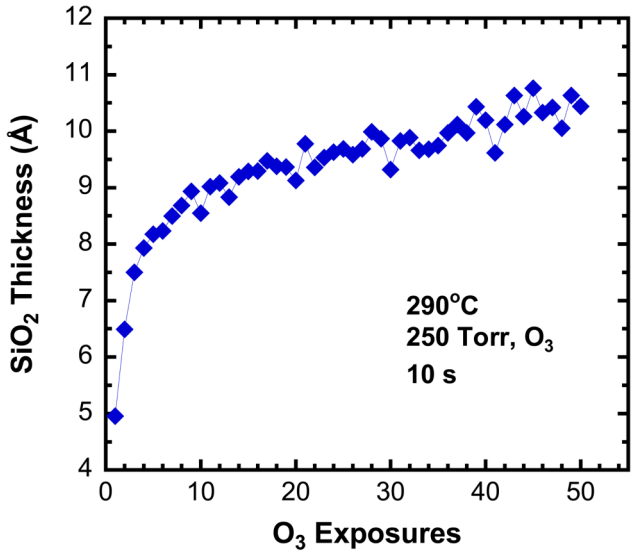

FIG. 14. SiO_2 thickness on Si_3N_4 surface vs number of O_3 exposures at 290 °C.

The self-limiting oxidation of Si_3N_4 observed in Fig. 14 is consistent with the surface oxide forming a diffusion barrier that restricts the progressive oxidation of the Si_3N_4 film. Similar behavior is observed during silicon oxidation when the SiO_2 layer forms a diffusion barrier that limits further oxidation.[64] The kinetics of silicon oxidation are modeled using the Deal–Grove model.[65] A similar model may apply for the oxidation of Si_3N_4 by ozone.

IV. CONCLUSIONS

Thermal Si_3N_4 ALE has been demonstrated using an oxidation and "conversation etch" mechanism using O_2 or O_3, HF, and TMA as the reactants. *In situ* spectroscopic ellipsometry measurements could simultaneously measure the thicknesses of the Si_3N_4 film and the SiO_2 layer on the Si_3N_4 film during thermal Si_3N_4 ALE. O_3 led to higher etch rates than O_2 at the same reactant pressures and exposures times. Etch rates of 0.25 and 0.47 Å/cycle were observed for O_2 and O_3, respectively, at 290 °C using an oxidant-HF-TMA reactant sequence. Using O_2 as the oxidant, the Si_3N_4 etch rates were only weakly dependent on O_2 pressure from 250 Torr to 450 Torr. Using O_3 as the oxidant, the Si_3N_4 etch rates were independent of the O_3 pressure from 37 to 250 Torr. The Si_3N_4 etch rate was dependent on the reaction sequence. The Si_3N_4 etch rate was reduced to 0.20 Å/cycle using an O_3-TMA-HF reactant sequence.

The Si_3N_4 etch rate decreased at lower temperatures. Using an O_3-HF-TMA reactant sequence, the Si_3N_4 etch rate decreased from 0.47 Å/cycle at 290 °C to 0.07 Å/cycle at 210 °C . The Si_3N_4 surface roughness was also reduced after Si_3N_4 ALE at 290 °C using an O_3-HF-TMA reactant sequence. An SiO_2 layer exists on the Si_3N_4 surface with a thickness of ~11 Å during the O_3-HF-TMA reactant sequence at 290 °C. This SiO_2 layer could be removed using sequential HF and TMA exposures. These sequential HF and TMA exposures can also very slowly etch the Si_3N_4 substrate.

Thermal Si_3N_4 ALE is similar to thermal Si ALE. Both thermal Si_3N_4 ALE and thermal Si ALE are performed using oxidation of their surfaces to form an SiO_2 layer. Subsequently, the SiO_2 surface layer is converted to Al_2O_3 or an aluminum oxide silicate by the TMA exposure. This converted surface layer is then fluorinated by HF. The AlF_3 or AlO_xF_y fluoride surface layer is then removed by a ligand-exchange reaction with TMA. The etch rates for thermal Si_3N_4 ALE and thermal Si ALE are fairly similar at 290 °C using either O_2 or O_3 as the oxidant. Thermal Si_3N_4 ALE should find utility for the fabrication of advanced semiconductor, optoelectronic, and MEMS devices.

ACKNOWLEDGMENTS

This research was funded by the Advanced Industries Accelerator (AIA) Program administered by the State of Colorado. The experimental apparatus was funded by the Defense Advanced Projects Agency (DARPA) under Grant No. W911NF-13-1-0041. The authors acknowledge Andrew Cavanagh for performing XPS survey scan measurements and Ryan Thorpe from Rutgers University for providing RBS and FRES analysis.

REFERENCES

[1]C. T. Carver, J. J. Plombon, P. E. Romero, S. Suri, T. A. Tronic, and R. B. Turkot, ECS J. Solid State Sci. Technol. **4**, N5005 (2015).
[2]K. J. Kanarik, T. Lill, E. A. Hudson, S. Sriraman, S. Tan, J. Marks, V. Vahedi, and R. A. Gottscho, J. Vac. Sci. Technol. A **33**, 020802 (2015).
[3]S. M. George and Y. Lee, ACS Nano **10**, 4889 (2016).
[4]Y. Lee and S. M. George, ACS Nano **9**, 2061 (2015).
[5]J. W. Coburn and H. F. Winters, J. Appl. Phys. **50**, 3189 (1979).
[6]K. J. Kanarik *et al.*, J. Vac. Sci. Technol. A **35**, 05c302 (2017).
[7]M. J. M. Vugts, G. L. J. Verschueren, M. F. A. Eurlings, L. J. F. Hermans, and H. C. W. Beijerinck, J. Vac. Sci. Technol. A **14**, 2766 (1996).
[8]T. Matsuura, J. Murota, Y. Sawada, and T. Ohmi, Appl. Phys. Lett. **63**, 2803 (1993).
[9]S. D. Park, K. S. Min, B. Y. Yoon, D. H. Lee, and G. Y. Yeom, Jpn. J. Appl. Phys. **44**, 389 (2005).
[10]H. Sakaue, S. Iseda, K. Asami, J. Yamamoto, M. Hirose, and Y. Horiike, Jpn. J. Appl. Phys. **29**, 2648 (1990).
[11]K. Suzue, T. Matsuura, J. Murota, Y. Sawada, and T. Ohmi, Appl. Surf. Sci. **82–83**, 422 (1994).
[12]R. J. Gasvoda, A. W. van de Steeg, R. Bhowmick, E. A. Hudson, and S. Agarwal, ACS Appl. Mater. Interfaces **9**, 31067 (2017).
[13]D. Metzler, R. L. Bruce, S. Engelmann, E. A. Joseph, and G. S. Oehrlein, J. Vac. Sci. Technol. A **32**, 020603 (2014).
[14]S. D. Park, W. S. Lim, B. J. Park, H. C. Lee, J. W. Bae, and G. Y. Yeom, Electrochem. Solid State Lett. **11**, H71 (2008).
[15]S. D. Park, C. K. Oh, J. W. Bae, G. Y. Yeom, T. W. Kim, J. I. Song, and J. H. Jang, Appl. Phys. Lett. **89**, 043109 (2006).
[16]K. S. Min, S. H. Kang, J. K. Kim, Y. I. Jhon, M. S. Jhon, and G. Y. Yeom, Microelectron. Eng. **110**, 457 (2013).
[17]D. S. Kim, J. E. Kim, W. O. Lee, J. W. Park, Y. J. Gill, B. H. Jeong, and G. Y. Yeom, Plasma Processes Polym. **16**, e1900081 (2019).
[18]J. W. Park, D. S. Kim, W. O. Lee, J. E. Kim, and G. Y. Yeom, Nanotechnology **30**, 085303 (2019).
[19]W. S. Lim *et al.*, Carbon **50**, 429 (2012).
[20]E. Vogli, D. Metzler, and G. S. Oehrlein, Appl. Phys. Lett. **102**, 253105 (2013).
[21]D. R. Zywotko, J. Faguet, and S. M. George, J. Vac. Sci. Technol. A **36**, 061508 (2018).
[22]Y. Lee and S. M. George, J. Phys. Chem. C **123**, 18455 (2019).
[23]J. C. Gertsch, A. M. Cano, V. M. Bright, and S. M. George, Chem. Mater. **31**, 3624 (2019).
[24]Y. Lee, J. W. DuMont, and S. M. George, ECS J. Solid State Sci. Technol. **4**, N5013 (2015).
[25]Y. Lee, J. W. DuMont, and S. M. George, Chem. Mater. **28**, 2994 (2016).
[26]Y. Lee, C. Huffman, and S. M. George, Chem. Mater. **28**, 7657 (2016).
[27]A. M. Cano, A. E. Marquardt, J. W. DuMont, and S. M. George, J. Phys. Chem. C **123**, 10346 (2019).
[28]Y. Lee, J. W. DuMont, and S. M. George, Chem. Mater. **27**, 3648 (2015).
[29]Y. Lee and S. M. George, J. Vac. Sci. Technol. A **36**, 061504 (2018).
[30]N. R. Johnson, H. X. Sun, K. Sharma, and S. M. George, J. Vac. Sci. Technol. A **34**, 050603 (2016).
[31]N. R. Johnson, J. K. Hite, M. A. Mastro, C. R. Eddy, and S. M. George, Appl. Phys. Lett. **114**, 243103 (2019).
[32]D. R. Zywotko and S. M. George, Chem. Mater. **29**, 1183 (2017).
[33]J. W. DuMont, A. E. Marquardt, A. M. Cano, and S. M. George, ACS Appl. Mater. Interfaces **9**, 10296 (2017).
[34]Y. Lee and S. M. George, Chem. Mater. **29**, 8202 (2017).
[35]N. R. Johnson and S. M. George, ACS Appl. Mater. Interfaces **9**, 34435 (2017).
[36]A. I. Abdulagatov and S. M. George, Chem. Mater. **30**, 8465 (2018).
[37]J. W. Clancey, A. S. Cavanagh, J. E. T. Smith, S. Sharma, and S. M. George, J. Phys. Chem. C **124**, 287 (2020).
[38]A. E. Kaloyeros, F. A. Jove, J. Goff, and B. Arkles, ECS J. Solid State Sci. Technol. **6**, P691 (2017).
[39]N. Posseme, V. Ah-Leung, O. Pollet, C. Arvet, and M. Garcia-Barros, J. Vac. Sci. Technol. A **34**, 061301 (2016).
[40]A. Kaushik, H. Kahn, and A. H. Heuer, J. Microelectromech. Syst. **14**, 359 (2005).
[41]N. Miyoshi, H. Kobayashi, K. Shinoda, M. Kurihara, T. Watanabe, Y. Kouzuma, K. Yokogawa, S. Sakai, and M. Izawa, Jpn. J. Appl. Phys. **56**, 06HB01 (2017).
[42]K. Shinoda, M. Izawa, T. Kanekiyo, K. Ishikawa, and M. Hori, Appl. Phys. Express **9**, 106201 (2016).
[43]K. Shinoda, N. Miyoshi, H. Kobayashi, M. Izawa, T. Saeki, K. Ishikawa, and M. Hori, J. Vac. Sci. Technol. A **37**, 051002 (2019).
[44]W. H. Kim, D. Sung, S. Oh, J. Woo, S. Lim, H. Lee, and S. F. Bent, J. Vac. Sci. Technol. A **36**, 01b104 (2018).
[45]C. Li, D. Metzler, C. S. Lai, E. A. Hudson, and G. S. Oehrlein, J. Vac. Sci. Technol. A **34**, 041307 (2016).
[46]M. Wang, P. L. G. Ventzek, and A. Ranjan, J. Vac. Sci. Technol. A **35**, 031301 (2017).
[47]Y. Ishii, K. Okuma, T. Saldana, K. Maeda, N. Negishi, and J. Manos, Jpn. J. Appl. Phys. **56**, 06hb07 (2017).
[48]K. Nakane, R. H. J. Vervuurt, T. Tsutsumi, N. Kobayashi, and M. Hori, ACS Appl. Mater. Interfaces **11**, 37263 (2019).
[49]S. D. Sherpa and A. Ranjan, J. Vac. Sci. Technol. A **35**, 01a102 (2017).
[50]S. D. Sherpa, P. L. G. Ventzek, and A. Ranjan, J. Vac. Sci. Technol. A **35**, 05c310 (2017).
[51]T. Matsuura, Y. Honda, and J. Murota, Appl. Phys. Lett. **74**, 3573 (1999).
[52]L. H. Liu *et al.*, J. Phys. Condens. Matter **28**, 094014 (2016).
[53]T. R. Gow, R. Lin, L. A. Cadwell, F. Lee, A. L. Backman, and R. I. Masel, Chem. Mater. **1**, 406 (1989).
[54]T. M. Mayer, J. W. Rogers, and T. A. Michalske, Chem. Mater. **3**, 641 (1991).
[55]T. Enomoto, R. Ando, H. Morita, and H. Nakayama, Jpn. J. Appl. Phys. **17**, 1049 (1978).
[56]I. Franz and W. Langheinrich, Solid-State Electron. **14**, 499 (1971).
[57]A. E. T. Kuiper, M. F. C. Willemsen, J. M. L. Mulder, J. B. O. Elferink, F. Habraken, and W. F. Vanderweg, J. Vac. Sci. Technol. B **7**, 455 (1989).
[58]H. H. Du, R. E. Tressler, K. E. Spear, and C. G. Pantano, J. Electrochem. Soc. **136**, 1527 (1989).
[59]HSC Chemistry (Software), Version 5.1, Outokumpu Research Oy, Pori, Finland, 2002.
[60]A. I. Abdulagatov and S. M. George (unpublished).
[61]H. Yao, J. A. Woollam, and S. A. Alterovitz, Appl. Phys. Lett. **62**, 3324 (1993).
[62]K. Utani, T. Suzuki, and S. Adachi, J. Appl. Phys. **73**, 3467 (1993).
[63]S. I. Raider, R. Flitsch, J. A. Aboaf, and W. A. Pliskin, J. Electrochem. Soc. **123**, 560 (1976).
[64]H. Z. Massoud, J. D. Plummer, and E. A. Irene, J. Electrochem. Soc. **132**, 2685 (1985).
[65]B. E. Deal and A. S. Grove, J. Appl. Phys. **36**, 3770 (1965).